 DOI: 10.1002/maco.200905536

Corrosion resistance of Ni-50Cr HVOF coatings on 310S alloy substrates in a metal dusting atmosphere

J. Saaedi*, H. Arabi, T. W. Coyle, S. Mirdamadi and H. Ghorbani

Metal dusting attack has been examined after three 168 h cycles on two Ni-50Cr coatings with different microstructures deposited on 310S alloy substrates by the high velocity oxy-fuel (HVOF) thermal-spray process. Metal dusting in uncoated 310S alloy specimens was found to be still in the initiation stage after 504 h of exposure in the 50H_2:50CO gas environment at 620 °C. Dense Ni-50Cr coatings offered suitable resistance to metal dusting. Metal dusting was observed in the 310S substrates adjacent to pores at the interface between the substrate and a porous Ni-50Cr coating. The porosity present in the as-deposited coatings was shown to introduce a large variability into coating performance. Carbon formed by decomposition of the gaseous species accumulated in the surface pores and resulted in the dislodgement of surface splats due to stresses generated by the volume changes. When the corrosive gas atmosphere was able to penetrate through the interconnected pores and reach the coating–substrate interface, the 310S substrate was carburized, metal dusting attack occurred, and the resulting formation of coke in the pores led to local failure of the coating.

1 Introduction

Carburization and metal dusting are degradation modes of high temperature alloys observed when the alloys are subjected to carbon-bearing environments, and have been widely experienced in chemical and petrochemical process facilities as well as fertilizer and nuclear power generation equipment [1, 2]. The term ''dusting'' is descriptive of the metal being converted to a powder mixture of carbon, carbides, metal, and oxides. Protection against metal dusting is possible mainly by formation of a dense, well-adherent oxide layer which allows no access of carbon-bearing gases to the metal surface.

In the CO–H_2 metal dusting environment, where the carbon activity is greater than unity and the oxygen partial pressure is sufficient for protective oxide formation in high chromium alloys, there is competition between (i) outward diffusion of chromium and formation of a Cr-rich oxide layer and (ii) the inward diffusion of C, formation of stable Cr containing carbides, and oversaturation. If the first process dominates, the alloy may be protected for a long time by the Cr-rich scale. If the second process prevails, a non-protective scale is formed and metal dusting initiates over wide areas and spreads rapidly [3].

Chromium oxide formation provides the most effective protection, and is favored by a high chromium concentration in the alloy and by a fine-grained microstructure or surface treatment which generates fast diffusion paths for the supply of chromium to the surface [3, 4]. Chromium oxide is impermeable to carbon, and so an adherent scale will protect an alloy from carbon attack. Thermal cycling damages the Cr_2O_3 scales, allowing gas access to the underlying alloy. Regrowth of the scale depletes the alloy surface of chromium, until the ability to reform Cr_2O_3 is lost. Carbon then dissolves in the alloys, precipitating chromium-rich carbides, and further lowering the matrix chromium concentration. Further reaction between the gas and the remnant chromium-depleted metal then leads to carbon deposition and metal dusting [5].

The empirical relationships developed by *Schueler* [6] and *Schillmoller* [7] give a lower alloying addition limit for effective metal dusting resistance in terms of the equivalent chromium concentration, Cr_{eq}. *Schillmoller* modified the equation proposed by *Schueler* to give: $Cr_{eq} = Cr\% + 3 \times (Si\% + Al\%) > 24$. Cr, Si, and Al can form protective oxide scales as Cr_2O_3, SiO_2, and Al_2O_3, respectively. As long as the protective oxide scale is maintained with no cracks or flaws, pits associated with metal dusting do not

J. Saaedi, T. W. Coyle
Centre for Advanced Coating Technologies, Department of Materials Science and Engineering, University of Toronto, 184 College Street, Toronto, Ontario M5S 3E4 (Canada)
E-mail: jahan.saaedi@utoronto.ca

J. Saaedi, H. Arabi, S. Mirdamadi, H. Ghorbani
Department of Materials and Metallurgical Engineering, Iran University of Science and Technology, Tehran (Iran)

appear. However, the oxide scales may crack at elevated temperature because of stresses caused by their growth and thermal cycles. Stresses that compress the oxide scale are sufficient to cause its spallation from austenitic stainless steels and nickel-base alloys. Once the scales have cracked pitting may or may not occur, depending on the competition between the attack of the carbonaceous gas and the healing of the oxide scales which in turn depends on the composition and reactivity of the exposed metal surfaces where the oxide scales are damaged [8].

Corrosion resistant coatings can be a cost effective alternative to changing the overall alloy composition, particularly for alloys with more than 30% chromium which are extremely difficult to fabricate by conventional hot working processes because of the development of a brittle alpha chromium phase. Once α-Cr is present, the alloy is more difficult to work because α-Cr is hard to deform and less ductile than γ-Ni. Furthermore, high chromium nickel-based alloys are susceptible to a decrease in ductility after exposure to elevated service temperatures due to the formation of α-Cr [9].

Modern thermal-spray processes such as high velocity oxy-fuel (HVOF) and plasma spraying are often used to deposit high chromium, nickel–chromium coatings on the surface of various parts to prevent high temperature oxidation and hot corrosion in gas turbines and other equipment [10]. During thermal spraying the heated and potentially molten, oxidized, or partially vaporized particles strike the substrate whereupon they deform (i.e., splat) and adhere through predominantly mechanical interlocking mechanisms [11]. The cooling rate of splats during the HVOF process is very high, typically in excess of 10^6 K/s for metals [12], which leads to formation of a fine-grained structure within splats. This may be favorable for protection against metal dusting by generating fast diffusion paths for the supply of chromium to the surface.

Thermal-sprayed coatings have been investigated for protection against metal dusting. *Rosado* and *Schütze* [13] compared several diffusion coatings on different substrates and also a γ-TiAl coating applied by HVOF on X10CrAl18 (at 400, 620, and 700 °C) and Alloy 800 substrates (at 400 °C) in 73%H_2, 25%CO, 2%H_2O, and an industrial atmosphere. The resistance of the HVOF coating to metal dusting attack was very good although coating failure was observed in the case of austenitic alloy 800 due to the large thermal expansion mismatch between the substrate and the coating. *Voisey* et al. [14] examined the corrosion resistance of plasma sprayed Alloy 800H (Ni-50Cr) coatings which contained high levels of unmelted particles and inter-connected porosity in a mixed gas environment of 80%CO, 20%H_2 at 650 °C. They reported that the coating had undergone metal dusting as well as significant spallation after 50 h of exposure. *Holland* [15] successfully used arc-spray and HVOF coatings of Ni-50Cr on 1Cr0.5Mo steel substrates in a metal dusting environment in a field application. He found that the arc-spray coating exhibited excellent protection against metal dusting damage in those areas where a continuous coating was present although localized spalling and detachment of the coating occurred at relatively sharp corners. Moreover, he found that the HVOF application process achieved superior coating integrity to the arc-spray process with only very minor and isolated delamination evident.

The work described in this paper is part of a larger study of the deposition and characterization of Ni-50Cr coatings, and presents mainly the metal dusting and carburization behavior of a Ni-50Cr/310S coating system after isothermal exposures. The research was intended to examine the potential of an HVOF corrosion resistant coating (50:50 Ni:Cr) to improve the metal dusting resistance of alloy 310S.

2 Experimental work

2.1 Materials

The coating material was a Ni-50Cr alloy (TAFA 1260F) powder with a particle size of −53/+20 μm purchased from Praxair (Eutectic Canada, Inc., Pointe Claire, Québec). The substrate was 310S stainless steel plate fabricated according to ASTM A240. The chemical compositions of the alloys are given in Table 1. The powder composition was measured by a Philips PW 2404 wavelength-dispersive X-ray fluorescence (WDXRF) spectrometer (C and O were taken from the powder supplier's data). The substrate composition was determined by a PMI-MASER spark emission spectrometer (WAS, Worldwide Analytical Systems GmbH, Uedem, Germany).

Both the alloys are expected to offer effective resistance to metal dusting according to the criteria of *Schueler* and *Schillmoller*.

2.2 Coating of coupons

There are a large number of processing variables in HVOF spraying, and the present samples were selected from the previously described [16] matrix of experiments, designed to identify the influence of process variables on the structure of the coatings. Two sets of HVOF process parameters were employed, selected to produce coatings with porosity levels and oxide contents of 2.5 vol% and 0.6 wt% for coating 1 and 0.8 vol% and 4.8 wt% for coating 2 (Table 2). Coating 1 had very low oxide content but higher levels of unmelted particles, and hence a relatively high porosity.

Each of the six sides of a coupon was coated using the same number of passes to obtain a coating thickness of ∼150 μm on each side. All samples for each of the two deposition conditions were coated simultaneously. Sharp edges are not generally

Table 1. The chemical compositions of used powder and substrate (wt%)

	Element											
	C	Cr	Fe	Ni	Si	Mn	Al	O	P	S	Mo	Others
Powder	0.041	48.1	1.0	Bal.	1.45	0.003	0.28	0.042	0.001	0.015	0.036	0.14
Substrate	0.05	25.7	Bal.	19.2	0.59	0.90			0.016	0.001	0.16	0.1

Table 2. Process parameter settings used for deposition of the powders

Coating	Parameter				
	Oxygen flow (SLM[a])	Propylene flow (SLM)	Air flow (SLM)	Stand-off distance (mm)	Feed rate (g/min)
1	136	96	354	300	60
2	208	104	354	300	60

[a]Standard liters per minute.

suitable for thermal spraying due to edge effects which limit coating performance. Hence the edges of the coupons were radiused before coating the side surfaces. The coupons had dimensions of 20 mm × 12 mm × 3 mm.

2.3 Exposure to the mixed gas environment

The gas mixture used for the metal dusting studies had a $50CO:50H_2$ composition. Previous research had reported that the rate of carbon transfer was maximized for $50CO:50H_2$ mixtures [17]. With this mixture, a reaction between the two gases will lead to the generation of water vapor at the metal dusting temperature. The metal dusting environment is characterized by carbon activities higher than unity and very low oxygen partial pressures. The pseudo-equilibrium carbon activity (by not allowing carbon to precipitate) and the oxygen partial pressure of the gas mixture were estimated at 620 °C. The carbon activities and oxygen partial pressures calculated from the reactions $CO + H_2 = C + H_2O$ and $2H_2 + O_2 = 2H_2O$ at 620 °C, assuming $P_{H2O} = 0.01$ atm, are $a_C = 71$ and $P_{O_2} = 3.17 \times 10^{-27}$ atm, respectively.

The specimen surface was mechanically ground, finishing with a 600-grit emery paper, followed by ultrasonic cleaning in ethanol. Samples were supported in quartz holders during exposure as shown in Fig. 1; each holder held one sample.

The metal dusting tests were performed in a horizontal tube furnace with a quartz retort chamber (100 cm length, 4.8 cm OD).

Figure 1. Test coupons in the quartz sample holders

Type 316 stainless steel (SS) flange endcaps with an O-ring seal were used to close the ends of the quartz retort tube. First the specimens were placed in the reaction tube which was sealed and flushed with argon in order to reach a low oxygen partial pressure, followed by flowing commercial-grade hydrogen. After reaching the required temperature, the mixture of H_2 and CO was introduced into the reactor. The gas feed system was equipped with three absorbers connected in series for removal of oxygen, water vapor, and light hydrocarbons in succession. The gas flow rate was fixed at 150 mL/min and the total pressure of the gas mixture was 1.3 atm. At intervals or after the required exposure time, the CO supply was shut off and the tube cooled to room temperature in flowing H_2 before the samples were removed. Prior and after exposure and also after ultrasonic cleaning each sample was weighed with a microbalance that could measure to ±100 μg.

Exposure periods at 620 °C were 168, 336, and 504 h. One specimen of each coating system or uncoated alloy was removed from the furnace for examination after each 168 h cycle, and replaced by a new specimen; the reactor was sealed again and the cycle repeated. The coupons of coating system 1 (C1), coating system 2 (C2), and uncoated 310S alloy were exposed simultaneously. Uncoated 310S alloy coupons were used as a reference for comparison with the coated 310S samples. To increase the sensitivity of the sample surface to pit initiation, we prepared a few specimens by scratching their surfaces before exposing them to the carburizing environment at 620 °C.

2.4 Mass difference measurements

At the intervals, the specimens were removed from the furnace for weight change measurement. Both the amount of coke deposition and the mass change of the specimen were measured after each exposure. Weight gain after reaction interval represented the total carbon uptake in the form of coke deposition and metal carburization, plus any oxidation. Because metal dusting is accompanied by carbon deposition, carbon pickup data provides some measure of the corrosion intensity based on the mass gain due to carbon dissolution and deposition. Net mass changes were assessed after mechanically removing the surface deposits, ultrasonic cleaning the specimens in ethanol, and then weighing the remaining substrate.

2.5 Sample examination

The surface of exposed specimens was assessed visually with the aid of a stereomicroscope. The morphology of carbon deposits was observed with a JEOL840A scanning electron microscopy (SEM). After removal of the deposits, the surfaces of the

specimens were examined by SEM and analyzed by X-ray diffraction (XRD) using a Philips PW1840 diffractometer with Cu Kα radiation and a scanning rate of 1.5° 2θ/min. Some specimens were mounted in cross-section, sectioned, and metallographically polished. Coating specimens were electro-etched in a solution of 10% oxalic acid at 1.2 V (uncoated specimens at 6 V). The microstructure and underlying damage to the metal surfaces were investigated using optical microscope (OM) and SEM. Before SEM investigation, the mounted samples were gold coated by sputtering. Energy dispersive X-ray spectroscopy (EDS) in the SEM was used to obtain qualitative and semi-quantitative evaluations of the changes in compositions in the reaction zones formed on some of the specimens.

3 Results

3.1 Surface studies

3.1.1 General features

After 168 h exposure the surfaces of the C1 specimen were blackened by carbon and a number of coke nodules were found on its plan surface and edges (Fig. 2a). Carbon deposition smoothly blackened all surfaces of the C2 specimen and partially blackened the surfaces of the uncoated 310S sample (Fig. 2b and c). Some small coke protrusions were noticed on the edges of these specimens.

After removing the non-adhesive powder carbon deposits by ultrasonic cleaning, the specimen's surfaces exhibited light green (for the coatings) and yellow (for the uncoated 310S) interference colors caused by oxidation (Fig. 2d–f). A number of small black spots were seen on the surface of the specimens but no pits were observed. The stability of the coatings and bonding of the coatings to the substrate was generally good. No cracks were observed on the C1 sample but a small amount of spallation of the coating had occurred at the corners. Further investigations showed that the coating in these areas was already thin because of extra grinding during preparation in order to radius the edge. A ~1 cm crack was observed at the intersection of the plan and side surfaces on one side of the C2 sample (Fig. 2e, upper-right). Small damaged areas were seen along the intersection of the plan and end surfaces of the C2 coating (arrows in Fig. 2e). Further investigation showed that the coating on the end surfaces in these areas was relatively thick (180 μm).

On the plan surface of the scratched sample of coating system 1, more coke protrusions were observed than had grown on the plan surfaces of unscratched samples. They were not uniformly dispersed over the surface, rather their formation was mainly restricted to an area close to the edge. After ultrasonic cleaning, a number of coating metal protrusions and eruptions were found in the areas where the coke protrusions occurred. They were formed along or near the scratches and the eruptions were filled with coke.

With increasing exposure time, 336 and 504 h, more and more carbon powder deposits covered the surfaces of the specimens; however, the short coke protrusions observed after 168 h along the edges of the specimens had not grown. A few new metal eruptions were observed on the plan surface of the C1 sample after 504 h of exposure underneath the coke protrusions (see arrows in Fig. 3a and b). These kinds of metal protrusions were not found on the surface of sample coating 2, but the corroded areas about 2 mm from the ends of the C2 specimen observed after 168 h were slightly larger after 504 h of exposure (Fig. 3c). The coke protrusions on the surface of the scratched sample of coating 1 were larger after 504 h of exposure.

In the case of the uncoated 310S alloy sample the number of black spots increased with further exposure (Fig. 4a). Moreover, damage was occasionally observed in the surface oxide layer (Fig. 4b).

3.1.2 Morphology of carbon deposits

Coke products which formed on the surface of coating 1 are shown in Fig. 5a and b. This type of coke formation is indicative of metal dusting corrosion. Bundles or nests of filamentous carbon were observed on the surface of coatings at higher magnifications

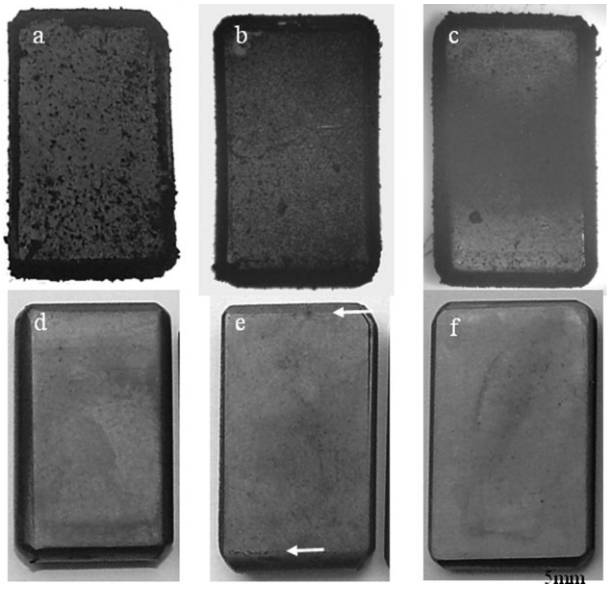

Figure 2. The surface morphologies of the C1 (a and d), C2 (b and e), and uncoated (c and f) specimens after 168 h exposure, (a)–(c) before, and (d)–(f) after ultrasonic cleaning

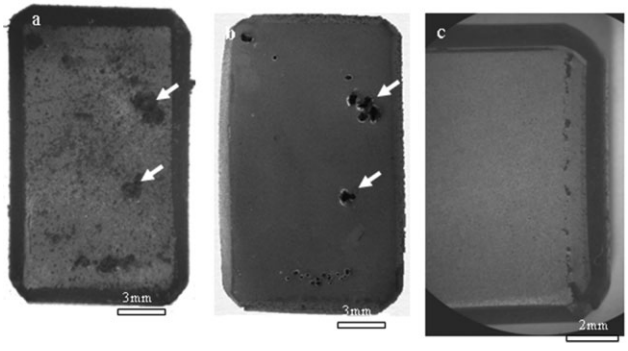

Figure 3. The surface morphologies of the coating system after 504 h exposure: (a) C1 sample before coke removing, (b) C1 sample after coke removing, and (c) C2 sample after coke removing

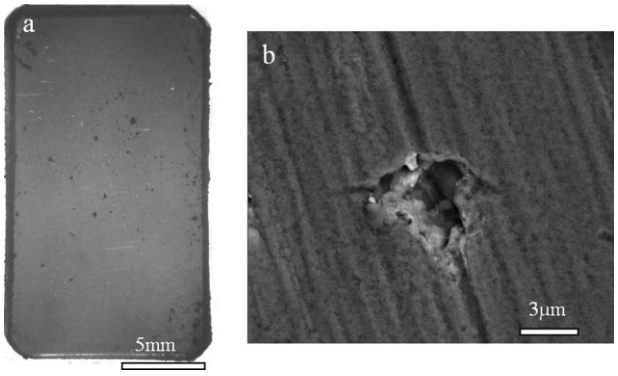

Figure 4. The surface morphology of the uncoated 310S sample exposed for 504 h showing: (a) the black spots and (b) a damage in the oxide layer

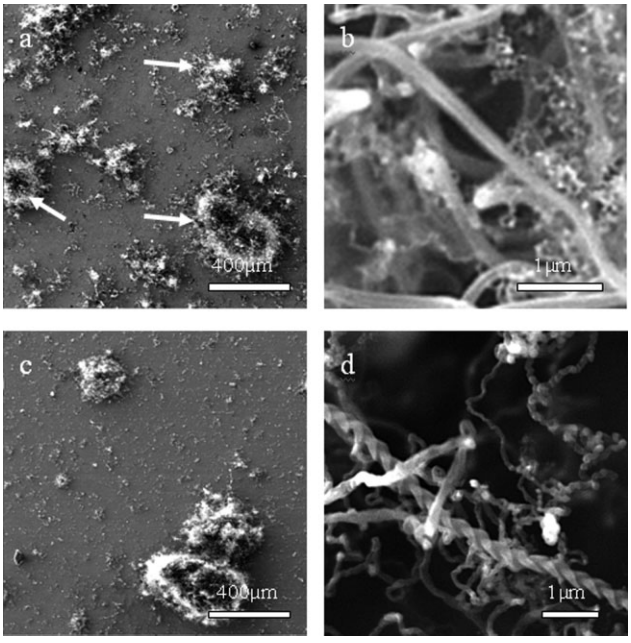

Figure 5. Carbon products formed on the surfaces of the specimens which were exposed for 168 h: (a) and (b) C1 sample, (c) and (d) uncoated sample

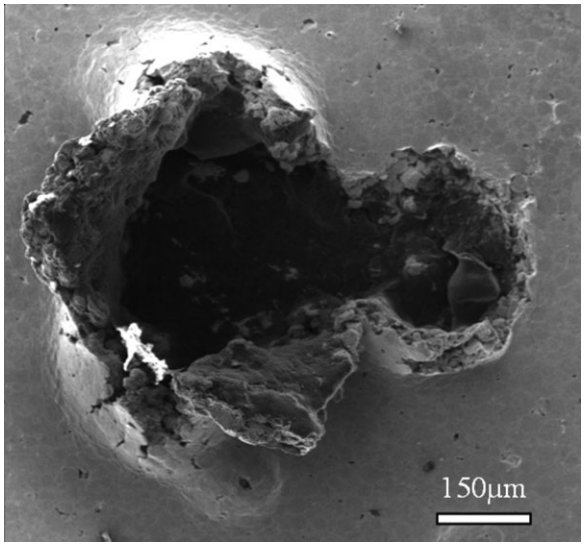

Figure 6. Local eruptions on the surface of coating 1 after 504 h exposure

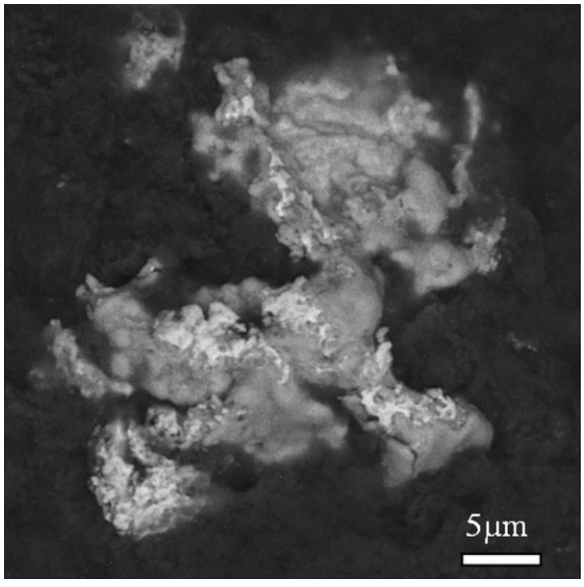

Figure 7. SEM image of a dislodged fragment embedded in the carbon deposits inside a damaged area on the surface of coating 1 after 504 h exposure

(arrows in Fig. 5a). These generally consisted of two different size filaments; some with a diameter in the range of 200–500 nm and carbon nanotubes and/or nanofibers with diameters less than 100 nm (Fig. 5b). The appearance of these filaments is consistent with growth via catalysis of carbon deposition by metallic nanoparticles at the filament tips.

Figure 5c and d presents images of coke products formed on the surface of an uncoated 310S sample. The coke bundles deposited on the surface of this specimen also included carbon fibers and carbon nanotubes and/or nanofibers. Fiber morphologies which were different than those seen on the surface of coatings were observed. Some of the fibers seemed to be made up of a string of spherical particles.

3.1.3 Analyses of corroded areas

Figure 6 shows higher magnification images of some of the metal protrusions observed on the plan surface of sample C1 in Fig. 3b. It seems that they developed following the formation of corrosion products in the subsurface pores, resulting in local eruptions through the coating due to stresses generated by the volume changes. Pre-existent surface pores are also visible in these figures, which provided paths for the penetration of the corrosive gas into the coating. The interior of the erupted areas was filled with coke. Dislodged metallic fragments embedded in the carbon deposits can be seen.

A backscattered electron (BSE) image of a metallic fragment inside the corroded area shown in Fig. 6 can be seen in Fig. 7. It

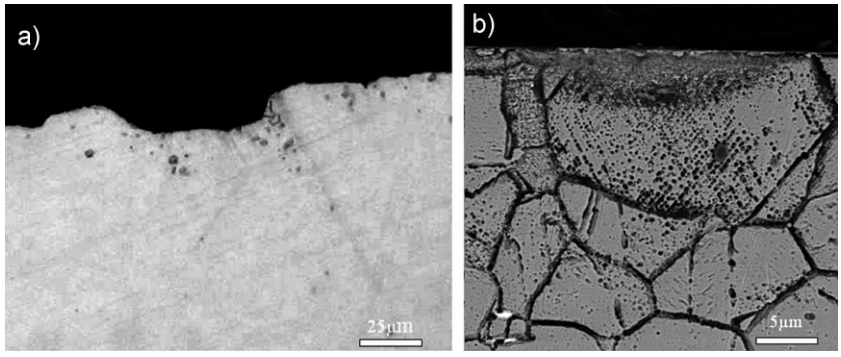

Figure 8. Metallographic cross-sections from the black spots which were formed on the surface of uncoated specimens for: (a) 504 h (optical micrograph), and (b) 168 h (BSE micrograph) exposures

had a size of 10–15 μm. Most of this fragment consisted of a light gray contrast phase and a white phase. An EDS semi-quantitative analysis of this particle showed that it consisted of 42Cr–31Ni–13O–9C–2.8Si–1.25Fe–0.52Al (wt%), indicating that this fragment had separated from the coating. The high O content would suggest that the light gray region is an oxide phase. The relatively high Si and Al contents in the chemical composition of this fragment may be associated with incorporation of these elements in the oxide. The size of the particle suggests that this fragment was part of an oxide layer on the surface of the original powder particle or which formed on a splat during deposition. The carbon detected is likely due to the surrounding carbon deposits.

3.1.4 Surface oxide characteristics

XRD and EDS analyses were performed on the ultrasonically cleaned plan surfaces of both the C1 and C2 coatings which had been exposed for 504 h. It was found that oxide films were formed on the surface of both coatings in the reducing exposure atmosphere.

Considering that the thicknesses of oxide layers were expected to be on the order of tens of nanometers, XRD would detect phases existing in the surface oxide layer along with the underlying alloy. Chromium oxide (Cr_2O_3) was the only oxide phase which was detected on both of the coatings' surfaces. Two metallic phases, fcc **γ**-Ni and bcc **α**-Cr, were identified which are the main constituents of the coating material. No carbide phases expected to be formed in the subsurface following metal dusting initiation were detected in these tests.

EDS analyses were also performed on the oxidized surfaces. The effective signal-producing depth for the performed EDS analysis is much less than that of XRD, but still larger than the thickness of the oxide layer expected. Therefore the EDS results also represent average compositions of the oxide layer and underlying phases. The semi-quantitative chemical compositions obtained were 55Cr–24Ni–17O–3.2Si–0.3Fe (wt%) for the C1 specimen and 58Cr–19Ni–19O–2.7Si–0.87C–0.2Fe (wt%) for the C2 specimen. The relatively high Si content indicated that it existed in the oxide layer, probably as silicon dioxide, together with chromium oxide although in too small a quantity to be detected by XRD. Chromia is impermeable to carbon and the detection of 0.87 wt% of carbon in the analysis of coating 1 was probably related to the carbon trapped in surface defects such as the pores seen in Fig. 6.

3.2 Cross-section studies

3.2.1 Uncoated 310S alloy

In areas where black spots were observed, the underlying damage was examined in cross-section. Metallographic cross-sections confirmed that the surface oxide film which was formed during exposure was rarely damaged and protected the underlying alloy against metal dusting attack over nearly the entire surface. The few black spots observed on the plan surface after ultrasonic cleaning were found to be very shallow, irregular pits which were filled with adherent carbon deposits and/or oxides (Fig. 8a). These spots were observed after 168 h of exposure but had still not developed into well-formed pits after 504 h.

A BSE image of a cross-section of another small black spot from the specimen exposed for 168 h can be seen in Fig. 8b. The pit was initiated near the center of a large grain. The damage did not extend more than one or two grains. Carburization of the grain and formation of carbide precipitates underlying the pit could be observed after etching of the cross-section.

3.2.2 Coating

OM investigations from cross-sections of C1 and C2 specimens after 168 h exposure showed that the coatings preserved the initial smooth surface topography in most areas. The surface damage was restricted to the large or interconnected pores (Fig. 9). Deposits of carbon products were observed inside these pores. The number of damaged spots on the surface of the C2 sample, which is the denser coating, was much less and their size was smaller than on the C1 sample.

Some of these pores had been completely filled with dense carbon deposits, which were not removed by the ultrasonic cleaning treatment. In some areas carbon ingress took place through the surface pores and penetrated into the intersplat pores. The formation of carbon deposits beneath or around surface splats led to deformation (Fig. 10) or separation (Fig. 11) of the splats.

There was no clear evidence of carburization of the coating alloy; no carbide precipitates were observed within the splats after etching (Fig. 12). The microstructure within the splats consisted of the fcc **γ**-Ni matrix with bcc **α**-Cr precipitates as expected from the equilibrium phase diagram and previously observed after heat treatment at 650 °C in a vacuum condition [18].

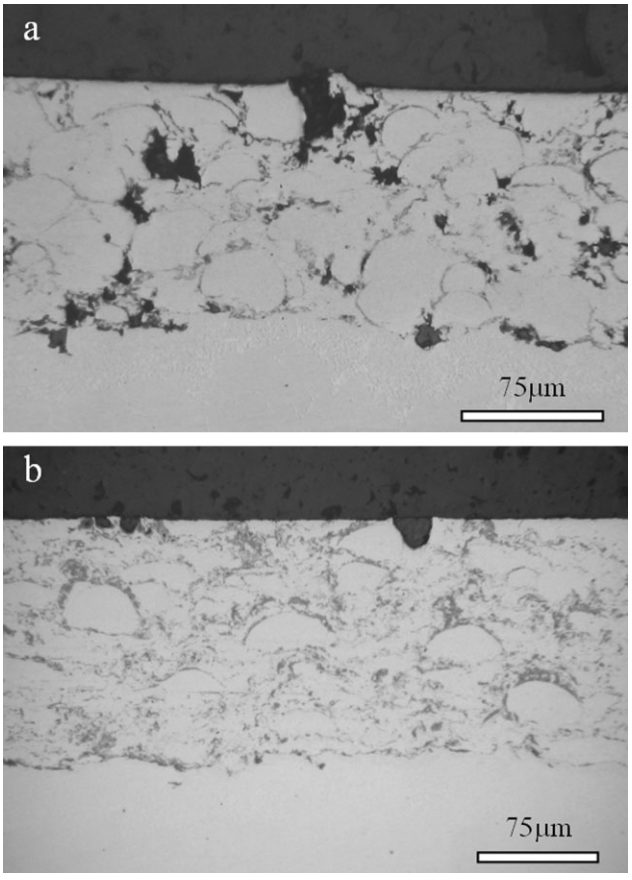

Figure 9. OM images of the coating systems after 168 h exposure: (a) C1 and (b) C2 samples

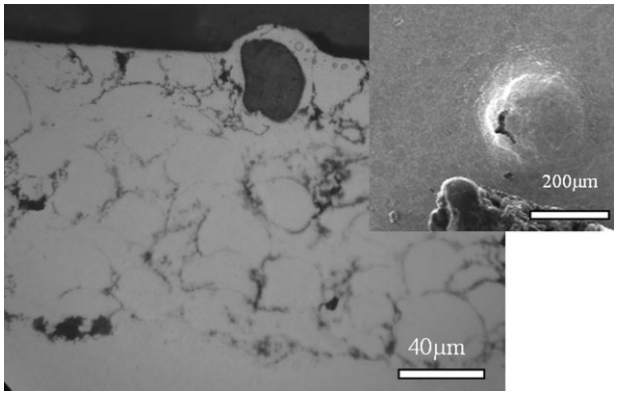

Figure 10. OM image showing the accumulation of carbon in a subsurface pore and deformation of the overlying splat in the C1 sample exposed for 504 h. A bulged area on the surface is seen in the small SEM image (upper-right)

3.2.3 Interface of coating and substrate

The OM and SEM analyses of the C1 specimens showed that carbon could deposit within surface and interconnected intersplat pores in the coating and at the coating/substrate interface. When carbon deposits formed at the interface the substrate was carburized. Two different morphologies of the MD degradation or

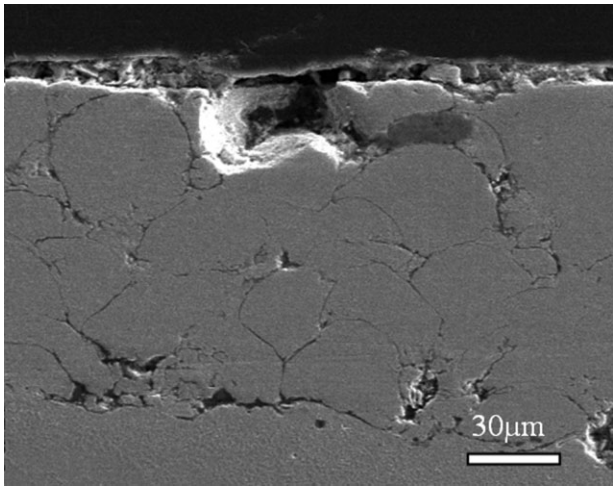

Figure 11. SEM image showing carbon deposits in intersplat pores and separation of a surface splat in the C1 sample exposed for 504 h

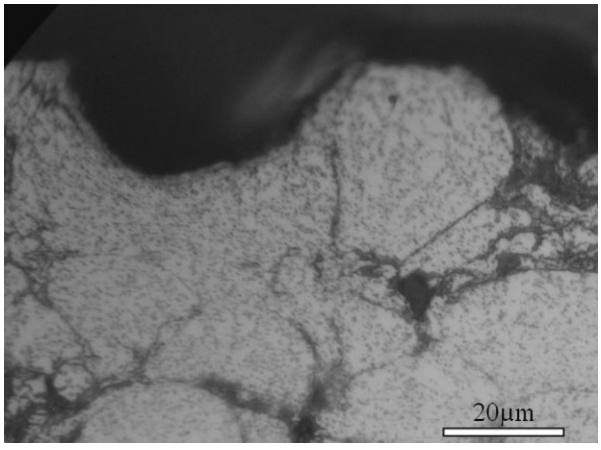

Figure 12. OM image after etching from a damaged area and underlying material of the C1 specimen exposed for 504 h

carburization products were observed on the substrate side of the interface after etching: a uniform structure about 50 μm in depth (labeled A in Fig. 13) which was also observed in C2 specimens, and a needle shaped or lamellar structure (labeled D in Fig. 13) under a non-etching white zone (labeled C in Fig. 13). Such structures (areas C and D) were not seen at the coating/substrate interface of the exposed C2 specimen. As mentioned above, the as-deposited C2 coating did not have an interconnected pore structure.

The extent of the areas of uniform structure and white zones in the interface of the C1 coating system increased with exposure time. Non-etching white zones were observed beneath extended coke-filled pores in the C1 specimens exposed for 336 and 504 h, area B in Fig. 13b. Formation of masses of coke inside these pores led to local eruptions in the coating surface and growth of coke protrusions on the surface (Fig. 14) in some areas. The reactant gases could reach the substrate through the pre-existing interconnected pore structure (or through pores which became

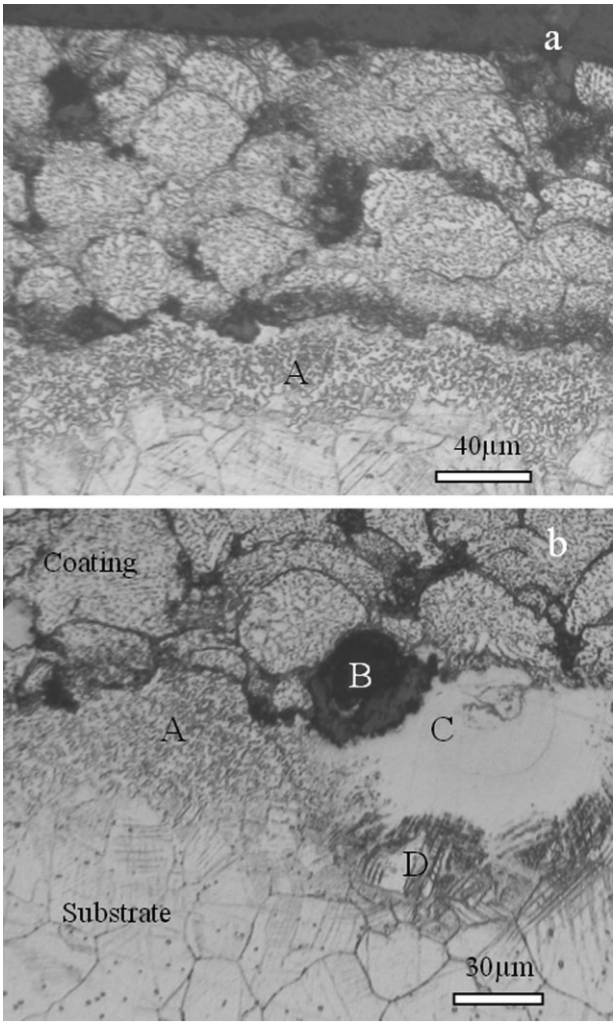

Figure 13. (a) Formation of a uniform interdiffusion structure in the substrate under the interface, area A, (b) a needle-like structure underlying a white zone beneath the extended coke-filled pore, areas C and D

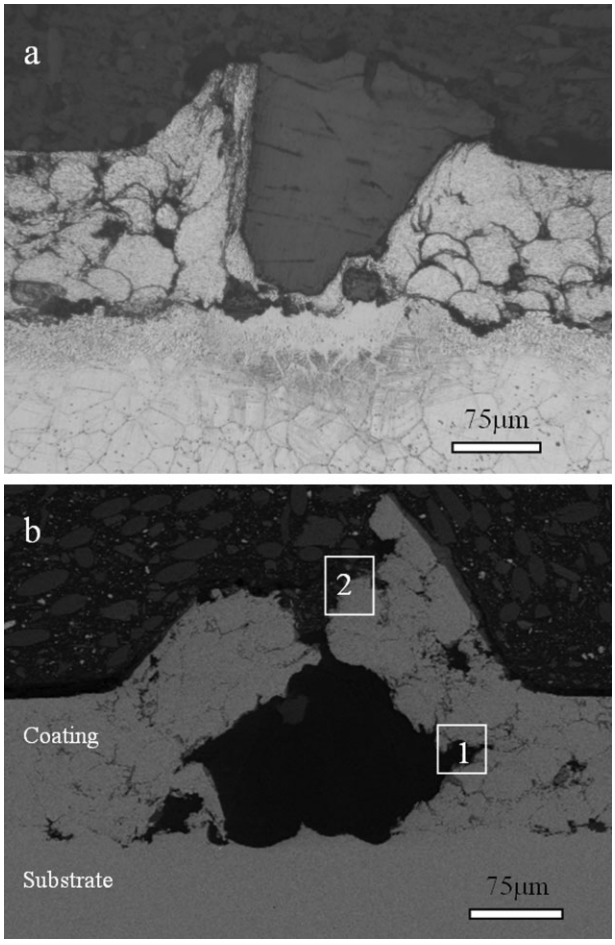

Figure 14. Formation of masses of coke inside the extended pores and eruption of coating surface in the C1 coating system after 504 h exposure, (a) OM image and (b) SEM image

interconnected during exposure). The formation of carbon deposits at the coating/substrate interface suggests that metal dusting of the substrate occurred, and that the stresses generated by the volume changes led to the eruptions observed in the coating surface.

Higher magnification SEM images of the areas B and C in Fig. 13b are shown in Fig. 15. The pores at the interface appear to grow into the substrate, as illustrated by the pore to the right of the non-etching zone (arrow in Fig. 15a). To the left of the non-etching zone a larger pore is seen in which an oxide layer covers the surface on the coating side (Fig. 15b). The pore surface on the substrate side was serrated due to corrosion. Tiny graphite and/or oxide particles which seem to have been dislodged from the non-etching zone adjacent to the corrosion front (arrow 1) can be seen in front of the serrated area in the higher magnification of the BSE image. The non-etching zone beneath the corrosion front includes a dispersion of fine precipitates (arrow 2).

A line scan analysis was performed normal to the coating–substrate interface, crossing the non-etching zone (narrow rectangle in Fig. 15a). As shown in Fig. 16, this indicated that the Cr content increased at the interface, but had been depleted to a depth of approximately 10 μm into the substrate and 5–10 μm into the coating. Ni was also depleted to a depth of ~10 μm into the substrate. A band of Fe was detected ~5 μm into the coating (the light areas). The dark bands in this Cr- and Ni-depleted areas of the substrate may be Cr- and/or Si-rich oxides. Although microstructural changes can be observed farther into the substrate, no changes in chemical composition were evident.

EDS analyses were performed on 25 μm × 30 μm areas in the non-etching zone and the needle-shaped or lamellar structure zone. The semi-quantitative results indicated that the non-etching zone had a composition of 69Fe–17Cr–12Ni–1.43C–0.38Si (wt%), while the lamellar structure zone had the composition of 53Fe–26Cr–18Ni–0.31C–0.78Si–1.14Mn (wt%). The average carbon content of the non-etching zone is about 4 times higher than in the lamellar structure zone. The Fe/Ni ratio in this zone is ~5.7, about 2 times that of the area farther from the interface.

Figure 17 shows a higher magnification image of the area of the coke-filled pore marked by the white square 1 in Fig. 14b. The EDS analysis of the area A in Fig. 17 found the composition to be predominantly C with a small amount of Fe (98.3C–1.7Fe (wt%)).

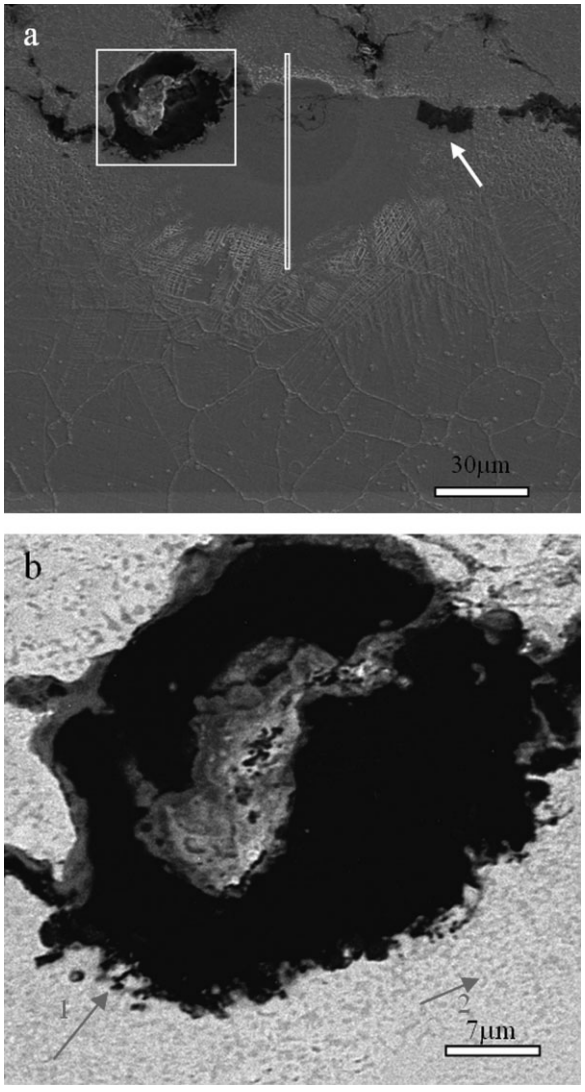

Figure 15. SEM images of an extended pore and underlying non-etching zone: (a) SE image and (b) BSE image of large rectangular area in (a)

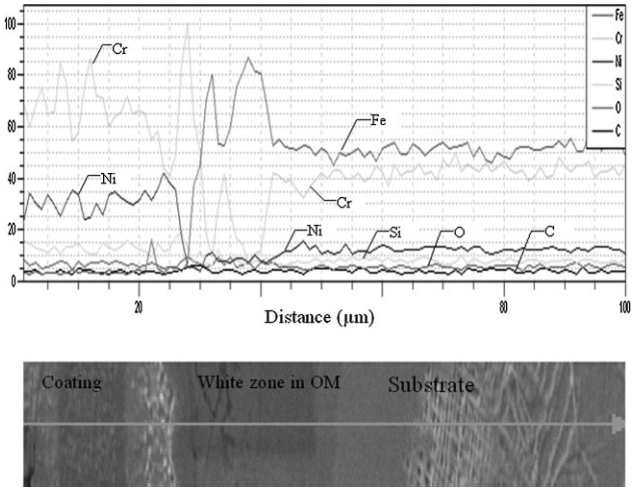

Figure 16. The EDS line scan analysis normal to the interface in the C1 specimen exposed for 504 h

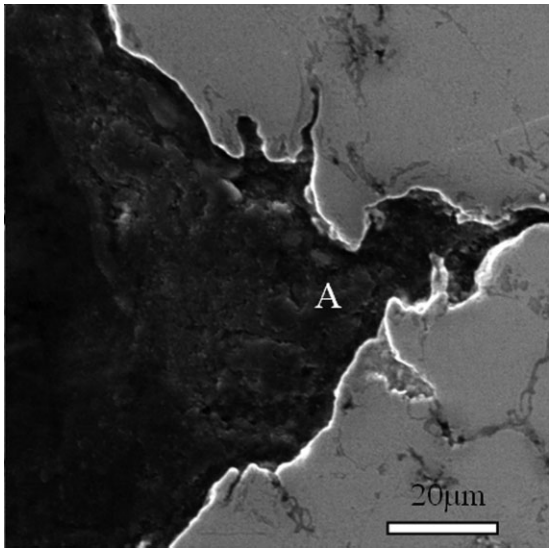

Figure 17. The area of the coke-filled pore marked by the white square 1 in Fig. 14b

Although this area of pore was relatively far from the substrate, the iron content within the coke indicates that these corrosion products must have resulted from degradation of the substrate.

A higher magnification image of the splat marked by the white square 2 in Fig. 14b is shown in Fig. 18. An oxide layer was clearly formed over all surfaces to which the atmosphere had access. A complex chemical composition for the oxide layer at A was found by EDS analysis (70Cr–13Ni–8O–3.2Si–2.7C–1.2Mn–0.9Fe (wt%)). It is thought that this analysis represents an average of a fine mixture of Cr- and Si-rich oxides, remnant metallic phases, and/or carbides. No clear evidence of carburization of the splat is observed.

3.3 Kinetic studies

The changes in weight of the specimens were obtained at intervals of 168, 336, and 504 h. Two different measurements are presented: (1) changes in weight of the specimens after the exposures and before ultrasonic cleaning (Fig. 19a) and (2) net mass changes which were obtained after ultrasonic cleaning of the specimens (Fig. 19b). The former was mainly due to the formation of external and internal (inside pores) carbon deposits. The latter did not include the loose and powder carbon deposits and so includes adherent surface deposits, internal carbon deposits, and carbon and/or oxygen dissolved into the alloy as well as weight loss due to spallation.

The mass gains were relatively moderate for the coating systems and uncoated 310S alloy, ranging between 1 and 2.5 mg/cm^2. The C2 coating system showed more mass gain than that of the C1 coating system in all intervals. This was consistent with the observations of the extent of surface blackening and formation of powdery carbon deposits. However, the coke protrusions on the edges and plan surfaces of the C2 coating

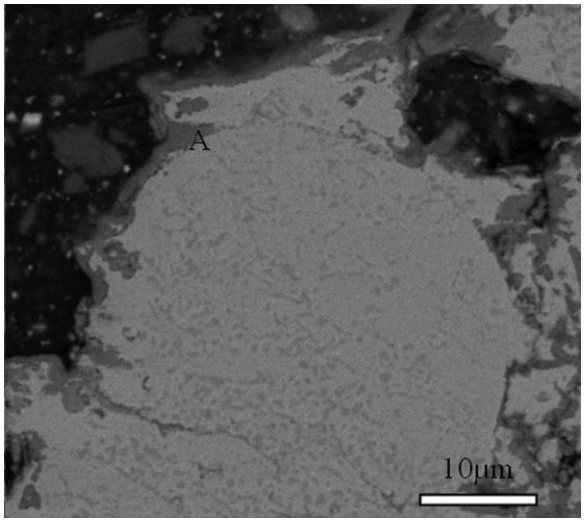

Figure 18. The area marked by the white square 2 in Fig. 14b

system were much shorter and less numerous than for the C1 coating. In general the weight gain trends did not exhibit the abrupt increase which is often encountered in metal dusting with longer exposure times. This indicated that metal dusting damage was not extensive in any of the specimens during the 504 h exposure. The positive net mass changes after ultrasonic cleaning of specimens confirmed the lack of significant spallation for all of the specimens (Fig. 19b).

The weight gains in the coated specimens were partly due to deposition of carbon products in the interconnected pores within the coating and inside the erupted areas. The weight increase due to oxidation/carburization and losses due to scale spallation and/or dusting may affect the net mass change results slightly. The net mass change of the C1 specimen was more than that of the C2 specimen. This could be related to the higher level of intrinsic porosity within coating 1 and therefore more deposition of corrosion products inside the pores.

4 Discussion

Exposure of all samples to the reactive atmosphere led to gradual blackening of the surfaces, which was mostly due to powder carbon deposition. The weight gains during exposure were largely due to this deposition. More carbon was deposited on the coated specimens than on the uncoated specimens, and the amount deposited on the C2 specimens was larger than on the C1 specimens, as determined from surface observations as well as weight changes. This may be related to the formation of $NiCr_2O_4$ spinel oxide in the microstructure of the Ni-50Cr coatings deposited by the HVOF method, as confirmed elsewhere [18]. The oxygen partial pressure in the carburization atmosphere was 3.17×10^{-27} atm, which is below the spinel stability level (Fig. 20). The oxide would be reduced according to the following reaction [19] producing Ni particles which are known to catalyze the onset of coking.

$$NiCr_2O_4 = Cr_2O_3 + Ni + 1/2O_2 \quad (1)$$

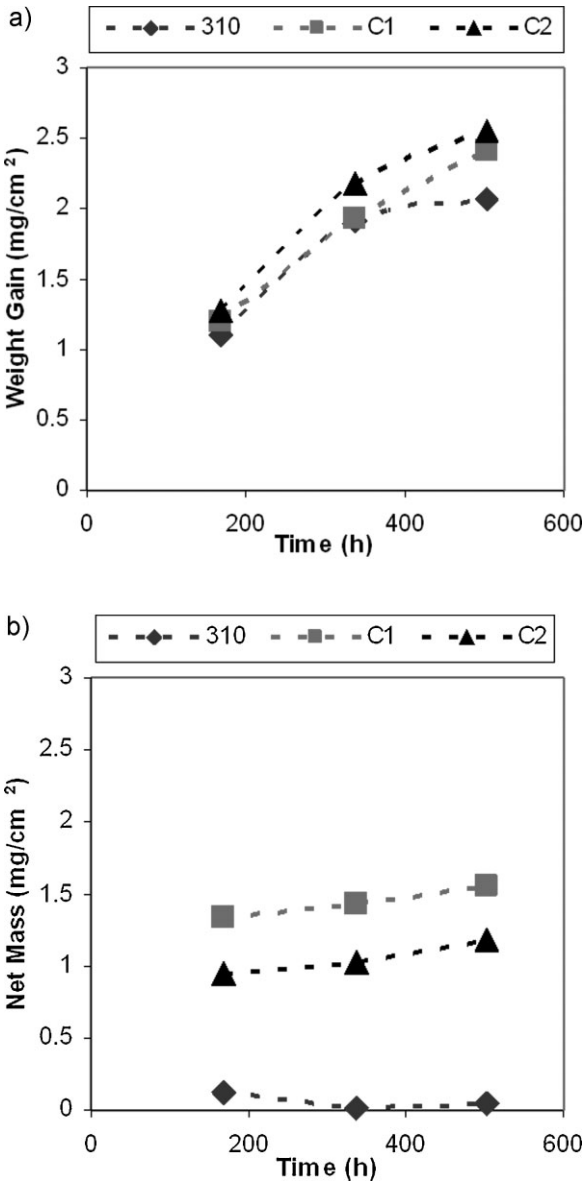

Figure 19. Graphical representation of the (a) weight gains and (b) net mass changes measured for the exposed coatings and uncoated 310S alloy specimens

Based on the initial chemical compositions of the substrate and coating given in Table 1, the Cr_{eq} (as defined by *Schillmoller* [7]) of the coating alloy would be ~53%, which is about 2 times the Cr_{eq} of the substrate alloy. Therefore the integrity of the protective oxide scale formed on the Ni-50Cr alloy would be expected to be higher than that formed on the 310S alloy because more scale-forming elements would be available to heal the protective oxide layer if any damage occurred. In the case of materials forming a protective oxide scale, metal dusting attack starts locally and often leads to formation of hemispherical pits and holes, from which coke grows in various forms [3, 20]. Oxide films formed on the surfaces of the coated and uncoated samples from the early stages of exposure as indicated by the interference colors, EDS results, and XRD patterns, consistent with the oxygen

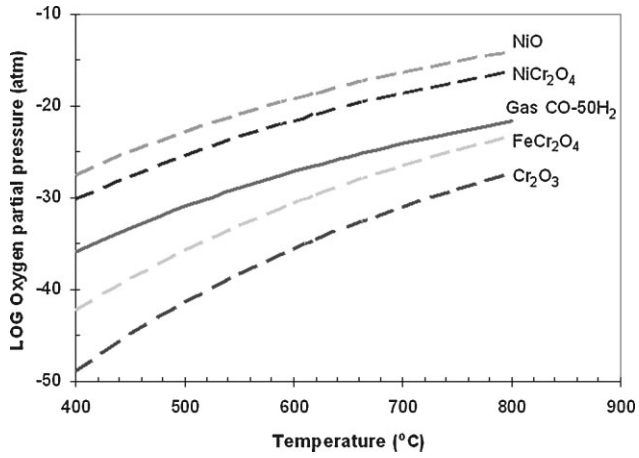

Figure 20. Thermal stability of spinels, Cr_2O_3, and NiO phases

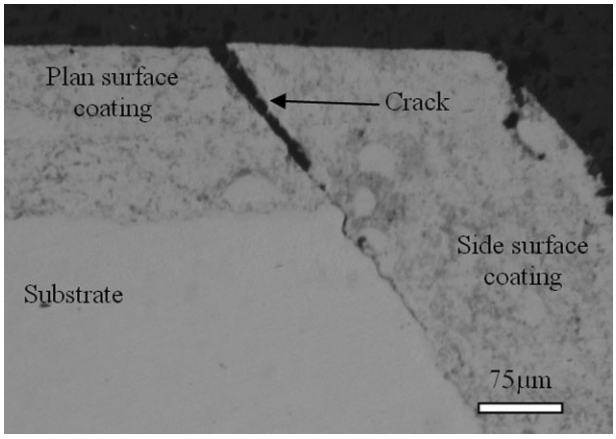

Figure 21. A crack formed at the interface of the plan and side surfaces of the C2 coating after 168 h exposure

partial pressure in the exposure environment (3.17×10^{-27} atm, see Fig. 20). Numerous small areas of thin localized carbon deposits (black stains or black spots) formed on all the specimens (Figs. 2d–f and 4a), but did not develop into the hemispherical pits generally associated with the beginning of metal dusting attack, even after 504 h of exposure.

The shallow craters under the black surface spots on the uncoated 310S alloy were contained within large grains beneath which numerous intragranular carbide precipitates were formed (Fig. 8b). The small coke nodules which formed over these spots included carbon fibers (Fig. 5c and d), indicating that metal dusting had initiated in these isolated locations, but had not fully developed after 504 h. This view is consistent with the observed weight change kinetics. Hence it could be said that the oxide film formed on the surface of the 310S alloy in an atmosphere with a CO/H_2 ratio of 1 protected the underlying alloy for at least 504 h. Thermal cycling is believed to accelerate the degradation due to the formation of cracks in the oxide film. There was no evidence that the three cycles down to RT during the 504 h exposure produced such an effect.

The C2 coating was very dense, which limited carbon penetration to pores located at the surface (Fig. 9b). The adhesion of this coating to the substrate was generally very good; no spallation occurred on the plan surfaces. However, a crack was observed near the intersection of the plan and side surfaces, where the coating thickness ranged from 150 to 180 μm (Fig. 21), probably due to stresses generated by the CTE mismatch between the substrate and coating. Defects in the coating were also observed in the plan surface near the end of the specimen where again the coating thickness was greater than 150 μm (Fig. 3c). At such defects, the reactive atmosphere penetrated the coating to reach the substrate. The attack of the substrate resulted in the damage seen on the coating surface after the 168 h exposure. These results indicate that the C2 coating system itself had not undergone metal dusting by 504 h.

The C1 coating had a higher porosity than the C2 coating before the exposure. Coke gradually deposited on the surface and inside the open pores from the early stages of exposure. Two types of coke form under metal dusting conditions. One type is formed homogeneously by gas phase reaction when the carbon activity is >1 and accumulates on the surface without participating in metal dusting. This carbon is poorly crystallized and does not diffuse into the metal. The second type of coke forms through catalytic action of metal particles, and usually consists of carbon nanotubes and/or nanofibers instead of powder [20, 21]. Most of the coke on the surface of the C1 coating was of the first type, and easily removed by ultrasonic cleaning. Small coke nodules or protrusions were formed in the larger pores and contained some filamentary carbon. Carbon deposits filled intersplat pores, resulting in separation of some surface splats due to stresses generated by the associated volume changes. However, no coke protrusions or eruptions developed from these intersplat pores. Moreover, no carbide precipitation was detected in the splats adjacent to the pores. These results indicate that, again, the coating itself did not undergo metal dusting even though carbon was deposited inside the pores.

The metallographic cross-sections of coating C1 revealed that the reactive atmosphere was able to reach the coating/substrate interface through the interconnected pores within the coating (Figs. 13–15). Semi-spherical non-etching white zones were observed adjacent to extended coke-filled pores which grew along the interface. Formation of this characteristic non-etching zone was accompanied by attack on the underlying steel, showing that the structure provided little or no protective effect. It seems that these areas were undergoing metal dusting.

The presence of continuous non-etching layers or bands under metal dusting pits in some Fe- and Ni-base alloys have been reported previously [22–25]. Two explanations of these layers have been proposed: (1) They are Cr-depleted carbide-free regions supersaturated with carbon and susceptible to metal dusting attack [22, 23] and (2) the zones contain a high number density of carbide particles [24, 25]. The non-etching zones in the present case did not form a continuous band under the damaged areas, but were relatively large, isolated areas with a depth greater than that of the interdiffusion layer. The discontinuous nature of the non-etching zones is most likely because the reactive atmosphere reached the substrate only at isolated locations.

BSE images of the area close to the corrosion front confirmed that fine precipitates were present in the non-etching zones (Fig. 15b), consistent with enhanced carbon transfer from the interfacial pore to the substrate. From a thermodynamic point of view carbides would form in distinct layers with increasing distance from the carbon source in the sequence M_3C_2, M_7C_3, and $M_{23}C_6$, depending on the local carburizing potential [25]. EDS line scans and area analyses revealed that a part of the non-etching zone was a high carbon area in which the Cr and Ni concentrations were significantly decreased. Internal oxidation was observed with the formation of chromium-rich and/or silicon oxides in the non-etching zone. The decrease of chromium and nickel in the white zone was probably due to migration of these elements toward the interface and their involvement in corrosion reactions lead to the formation of oxides in the interconnected pores. BSE imaging from the serrated surface of the pore revealed the formation of flakes of oxide and/or graphite at the corrosion front (Fig. 15b). The formation of oxide or graphite in this way would be accompanied by volume changes which would lead to disintegration of the surface of the metal grain, the mechanism of attack proposed for high alloy metals [22, 25–28]. The formation of small metallic particles would in turn catalyze deposition of graphite and may therefore explain the formation of coke in the pores that eventually led to local eruptions on the coating surface.

It is interesting to note that the uncoated 310S alloy was quite resistant to attack under the exposure conditions, but the alloy was sensitive to metal dusting as the substrate beneath the Ni-50Cr coating. The nature of the surface of the uncoated specimens (ground and rinsed with acetone) prior to exposure would have been essentially identical to the surface of the substrates before deposition (grit blasted and rinsed with acetone). Detailed microstructural studies revealed no detectable changes to the surface of the substrates at the coating interface after deposition [29]. A continuous oxide scale was observed on the free surface of the uncoated 310S alloy after exposure; there were no carbides evident under the scale. However, no oxide layer was evident on the substrate surface within pores at the substrate–coating interface of C1 samples and a dense dispersion of carbides was observed in the non-etching zones in the substrate adjacent to the surface of the interfacial pores. A protective layer of Cr_2O_3 did form on the coating surface of these interfacial pores, indicating that the higher chromium content of the coating still provided protection under the conditions present in the pore. The substrate of the C2 coating experienced higher temperatures during deposition, and would therefore be more likely to have seen changes in its surface chemistry and structure. If the substrate attack at the substrate–coating interface was related primarily to surface damage during deposition, we would expect the C2 substrates to be more susceptible to attack than the C1 substrates. However, the substrate attack was only observed under the C1 coatings, adjacent to pores through which gaseous environment had access.

The environment present inside the interfacial pores is clearly different than that at the free surface of the sample. It is well known that metal dusting attack is accelerated when the reactive gas atmosphere is stagnant [30, 31]. It may be useful to consider the interfacial pores as isolated from the exterior flowing gaseous environment when considering possible reaction mechanisms. Reaction products may build-up within the pores, changing the relative rates of competing reactions. In the free flowing reactive atmosphere, the water content was assumed to be $V_{H_2O} \approx 1\%$ at 620 °C, resulting in a C activity of $a_C \approx 71$ for a H_2:CO ratio of 1:1. Within the interfacial pore the large amount of C present would set the C activity at $a_C = 1$. Considering the

$$CO + H_2 \leftrightarrow C + H_2O \quad (2)$$

equilibrium, a decrease in the C activity should result in an increase in the H_2O vapor pressure within the isolated pore relative to the free flowing gas atmosphere. This may change the nature of the oxide scale formed on the substrate alloy. *Gibbs* [32] has proposed that the development of a catalyst for the Boudouard reaction, $2CO = CO_2 + C$, within the scale leads to deposition of carbon by CO within the oxide layer which split open the scale and left the system in a state of rapid ''breakaway'' oxidation. A comparison between different steels oxidized in wet and in dry CO_2 at 500 °C showed that the presence of water vapor leads not only to increased oxidation rates but also to greater percentages of carbon [33]. In the presence of water vapor the rate of breakaway oxidation and the amount of carbon in the scale were increased.

5 Conclusions

- 310S alloy was found to have a good resistance to metal dusting as a result of the formation of a protective oxide film in the mixed gas environment of $50CO–50H_2$ at 620 °C to the maximum exposure time of 504 h. Black spots were seen on the surface of uncoated 310S alloy specimens but these did not become significant metal dusting pits after three 168 h cycles. In a few isolated areas, where the oxide film was damaged, carbide precipitates were formed inside large surface grains, indicating the initiation of dusting. The resistance of this alloy to longer-term exposures deserves further study.
- The HVOF Ni-50Cr coating itself did not exhibit metal dusting in this severe corrosive environment. However, large and interconnected pores present in as-deposited coatings limit the protection provided to the substrate and introduce a large variability into coating performance.
- A larger amount of powdery C formed on the surface of the coated specimens than on the uncoated specimens, perhaps due to the catalyzing effect of Ni in the coatings, produced by reduction of pre-existent $NiCr_2O_4$ spinel in the coatings.
- The premature failure or spallation of the coating was observed when the thickness of the coating exceeded ~150 μm or when defects were present at the coating–substrate interface or within the coating. The latter defects were typically associated with the difficulty of depositing the coating around sharp corners and edges of the substrate.
- Carbon was deposited in the surface connected pores. The stresses generated by the volume changes due to oxidation and/or graphite formation inside the pores in some cases pushed the surface splats away from the coating.

- Carbon was deposited throughout the interconnected pore channels, including pores located at the coating–substrate interface. Carbon diffused into the substrate underneath interface pores resulting in carburization of the 310S alloy to a depth of about 50 μm below the coating–substrate interface. A non-etching zone formed underneath the large interface pores which contains a high number density of carbide precipitates in a Cr-depleted matrix.
- The non-etching zone suffered metal dusting attack, showing that the structure provided little or no protective effect. The dusts which dislodged from the surface of this area catalyzed graphite deposition resulting in accumulation of coke inside the pore. The stresses generated by the volume changes in and around the interfacial pores led to local failures of coating in the form of eruptions on the coating surface.
- The surface of the uncoated 310S alloy was more resistant to metal dusting attack when exposed directly to the free flowing gaseous corrosive atmosphere than was the surface of the 310S substrate adjacent to the interfacial pores. This must be attributed to changes in the composition of the corrosive gas mixture within the nearly isolated pores.

Acknowledgements: Thanks are expressed to Research Institute of Petroleum Industry, Tehran, Iran for help with corrosion tests and the Centre for Advanced Coating Technologies, University of Toronto, Toronto, Canada, for help with deposition of the coatings.

6 References

[1] R. Yin, *Mater. Sci. Eng. A* **2005**, *391*, 19.
[2] C. M. Chun, T. A. Ramanarayanan, *J. Electrochem. Soc.* **2007**, *154*, C465.
[3] H. J. Grabke, *Mater. Corros.* **1998**, *49*, 303.
[4] H. J. Grabke, R. Krajak, E. M. Muller-Lorenz, S. Strauss, *Mater. Corros.* **1996**, *47*, 495.
[5] D. J. Young, *Mater. Sci. Forum* **2006**, *522–523*, 15.
[6] R. C. Schueler, *Hydrocarbon Process.* **1972**, *51*, 73.
[7] C. M. Schillmoller, *Chem. Eng.* **1986**, *93*, 83.
[8] Y. Nishiyama, K. Moriguchi, N. Otsuka, T. Kudo, *Mater. Corros.* **2005**, *56*, 806.
[9] D. A. Shifler, L. K. Kohler, *CORROSION/2000*, NACE, Houston, USA, **2000**, Paper No. 00242.
[10] J. Tuominen, P. Vuoristo, T. Mäntylä, S. Ahmaniemi, J. Vihinen, P. H. Andersson, *J. Therm. Spray Technol.* **2002**, *11*, 233.
[11] K. Luer, J. Du Pent, A. Marder, *CORROSION/1999*, NACE, Houston, USA, **2001**, Paper No. 298.
[12] J. R. Davis, (Ed.), *Handbook of Thermal Spray Technology*, ASM International, Materials Park, OH **2004**, p. 3.
[13] C. Rosado, M. Schütze, *Mater. Corros.* **2003**, *54*, 831.
[14] K. T. Voisey, Z. Liu, H. Zougdani, F. H. Stott, *Mater. Sci. Forum* **2004**, *461–464*, 553.
[15] M. L. Holland, *CORROSION/2001*, NACE, Texas, USA, **2001**, Paper No. 01385.
[16] J. Saaedi, T. W. Coyle, H. Arabi, S. Mirdamadi, J. Mostaghimi, *J. Therm. Spray Technol.* **2010**, *19*, 521.
[17] C. M. Chun, J. D. Mumford, T. A. Ramanarayanan, *J. Electrochem. Soc.* **2002**, *149*, B348.
[18] J. Saaedi, T. W. Coyle, S. Mirdamadi, H. Arabi, J. Mostaghimi, *Surf. Coat. Technol.* **2008**, *202*, 5804.
[19] D. J. Young, *High Temperature Oxidation and Corrosion of Metals*, 1st Ed., Elsevier Ltd, Oxford **2008**, Chapter 10.
[20] Z. Zeng, K. Natesan, V. A. Maroni, *Oxid. Met.* **2002**, *58*, 147.
[21] K. Natesan, Z. Zeng, *Final Project Report, Energy Technology Division*, Argonne National Laboratory, Illinois, USA, **2003**, p. 26.
[22] P. Szakalos, R. Pettersson, S. Hertzman, *Corros. Sci.* **2002**, *44*, 2253.
[23] S. Strauβ, R. Krajak, H. J. Grabke, *Mater. Corros.* **1999**, *50*, 622.
[24] B. A. Baker, G. D. Smith, *presented at International Workshop on Metal Dusting*, ANL, Argonne, Illinois, *USA, September 26–28,* **2001**.
[25] J. Z. Albertsen, *Ph.D. Thesis, Norwegian University of Science and Technology, Norway*, **2007**, p. 123.
[26] J. Klöwer, H. J. Grabke, E. M. Müller-Lorenz, *Mater. Corros.* **1998**, *49*, 328.
[27] P. Szakalos, *Mater. Corros.* **2003**, *54*, 752.
[28] P. Szakalos, M. Lundberg, R. Pettersson, *Corros. Sci.* **2006**, *48*, 1679.
[29] J. Saaedi, *Ph.D. Thesis*, Iran University of Science and Technology, *Iran,* **2009**.
[30] J. R. Davis (Ed.), *ASM Specialty Handbook, Stainless Steels*, ASM International, Materials Park, OH **1994**, p. 217.
[31] J. R. Davis (Ed.), *Heat-Resistant Materials*, ASM International, Materials Park, OH **1997**, p. 169.
[32] G. B. Gibbs, *Oxid. Met.* **1973**, *7*, 173.
[33] A. M. Pritchard, J. E. Antill, K. R. J. Cottell, K. A. Peakall, A. E. Truswell, *Oxid. Met.* **1975**, *9*, 181.

(Received: September 26, 2009) W5536
(Accepted: December 10, 2009)